Geol. Mag. **147** (*4*), *2010, pp. 497–507. © Cambridge University Press 2010*
doi:10.1017/S001675680999077X

Viscosity estimates of salt in the Hormuz and Namakdan salt diapirs, Persian Gulf

SOUMYAJIT MUKHERJEE*†, CHRISTOPHER J. TALBOT‡ & HEMIN A. KOYI‡

*Department of Earth Sciences, Indian Institute of Technology Bombay, Mumbai-400 076, Powai, India
‡Hans Ramberg Tectonic Laboratory, Uppsala University, 752 36 Uppsala, Sweden

(*Received* 10 March 2009; *accepted* 8 October 2009; First published online 15 January 2010)

Abstract – The parabolic surface profiles of the Hormuz and Namakdan salt diapirs in the Persian Gulf suggest that they have been extruding with Newtonian viscous rheologies for the last 10^4 years. We derive velocity profiles for these diapirs, neglecting gravitational spreading and erosion/dissolution while assuming incompressible Newtonian rheology of the salt. Fitting known rates of extrusion at specific points in its elliptical cross-section, the dynamic viscosity of the salt of the Hormuz diapir is found to range between 10^{18} and 10^{21} Pa s. Approximating its sub-circular cross-section to a perfect circle, the range of viscosity of the salt of the Namakdan diapir is obtained as 10^{17}–10^{21} Pa s. These calculated viscosities fall within the range for naturally flowing salts elsewhere and for other salt diapirs but are broader than those for salts with Newtonian rheology deforming at room temperatures. The salts of the Hormuz and Namakdan diapirs are expected to exhibit a broader range of grain size, which matches the limited existing data.

Keywords: Hormuz diapir, Namakdan diapir, salt diapir, viscosity, Newtonian viscous fluid.

1. Introduction

Measuring or constraining the rheological parameters of rocks is of fundamental importance in materials science and structural geology. Rocks under stress for thousands of years due to tectonic forces can undergo ductile deformation. However, parameters of ductility of rock units, most notably the dynamic viscosity (henceforth referred to as 'viscosity'), are not always possible to measure in the laboratory. One of the indirect approaches to constraining mantle viscosity in the past few decades has been to study crustal rebound rates (as reviewed by Schubert, Turcotte & Olson, 2001). Although the viscosities of rocks should ideally decrease with depth due to increase in temperature, single representative values of the parameter for particular rock types have often been preferred by previous workers (e.g. Talbot *et al.* 2000) and have proved useful in tectonic modelling (e.g. Schultz-Ela & Walsh, 2002).

In map view, salt diapirs are usually circular to elliptical salt structures. Rayleigh-Taylor instability (rise of lighter salt through superjacent denser rocks due to buoyancy) is suggested as one of the mechanisms for the formation of salt diapirs (e.g. Price & Cosgrove, 1990; Davies, 1999). In this case, both the salt and the country rock are taken as viscous fluids over a long geological time span (as per Turcotte & Schubert, 2002). However, several other mechanisms of salt diapirism do exist (e.g. faulting of overburden units by thin- or thick-skinned extension, differential loading, erosion of the crest of salt-cored anticlines: Koyi, 1991*b*; Vendeville & Jackson, 1992; Koyi, Jenyon & Petersen, 1993; Weijermars, Jackson & Vendeville, 1993; Jackson, Vendeville & Schultz-Ela, 1994; Koyi, 1997; Sans & Koyi, 2001; Koyi *et al.* 2008, among others).

Most of the 200 or so diapirs of Hormuz salt in the Zagros Mountains of Iran (e.g. De Böckh, Lees & Richardson, 1929; Kent, 1958; Harrison, 1930, 1931; Bosák *et al.* 1998 and their review; A. Bahroudi, unpub. Ph.D. thesis, Uppsala University, 2003 and references therein), with diameters ranging from 1 to 15 km (Bruthans *et al.* 2009), extrude majestic mountains of salt that rise 400 m above their vents in limestones (Talbot, 1998). Halite (NaCl) is the main constituent (up to 96 wt %) of these salts (Bruthans *et al.* 2008) and shows minor differences in colour (Talbot, Aftabi & Chemia, 2009). The minor constituents in the halite are oxides of sodium, magnesium, aluminium, silicon, potassium, calcium and iron, and also anhydrides (Bruthans *et al.* 2008; Talbot, Aftabi & Chemia, 2009; Talbot, Farhadi & Aftabi, 2009). Fragments of sedimentary (sandstone, limestone, dolostone, shale, siltstone), igneous (rhyolite, andesite, ignimbrite, trachyte, granite, gabbroic rocks, metaphyres, tuffs) and metamorphic rocks (schists, gneisses, metabasites, quartzite), with sizes varying from less than a millimetre up to 2 km within these diapirs, are also present, with a few oriented along the foliation planes. The mélange of inclusions are either pieces of the basement rocks or are syn-Hormuz depositions (Jahani *et al.* 2007 and references therein). In places the igneous rocks are extensively kaolinitized (Talbot, Aftabi & Chemia, 2009). In addition, the diapirs are covered in some places with vegetation, and a few centimetres to tens of metres of surficial weathered deposits of intermediate composition, including evaporite (gypsum, anhydrite, minor halite), carbonates and silicate oxides (chiefly

†Author for correspondence: soumyajitm@gmail.com

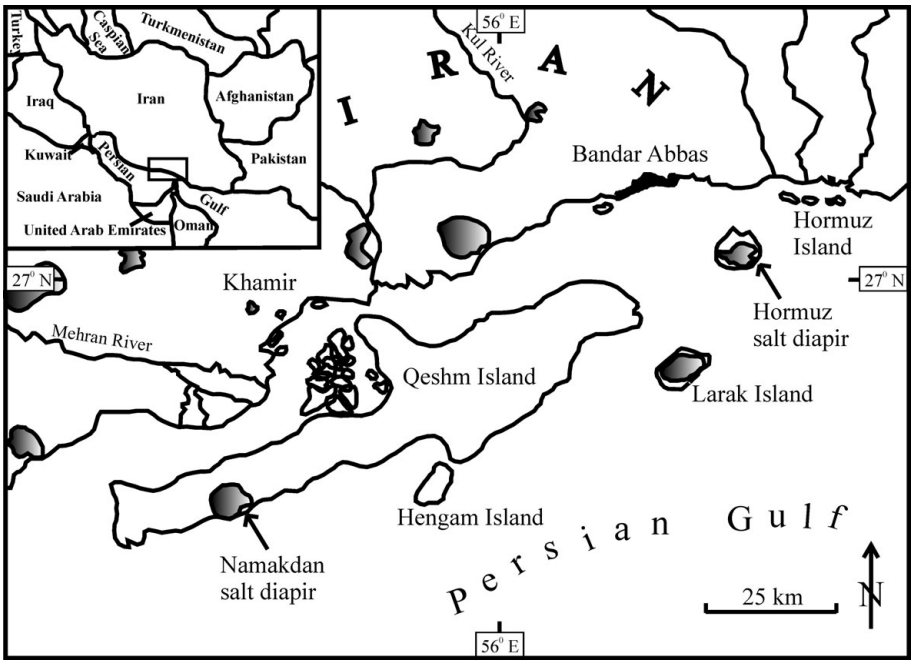

Figure 1. Geographic locations of the Hormuz and Namakdan diapirs in the Persian Gulf. Dark areas represent exposed salts of the diapirs. Reproduced with permission from Bruthans, J. *et al.* 2006. Holocene marine terraces on two salt diapirs in the Persian Gulf, Iran: age, depositional history and uplift rates. *Journal of Quaternary Science* **21**, 843–57, Wiley-Blackwell.

quartz, phyllosilicates and hematite) in other places (Kent, 1958; Bruthans *et al.* 2009). The residual soils in the Hormuz diapir are marl-rich and limonitic, and consist of anhydrite crystals (Talbot, Aftabi & Chemia, 2009). The near-surface rocks of the Hormuz diapir are affected by low-angle thrusts and sub-vertical tear faults (Talbot, Aftabi & Chemia, 2009). The two diapirs considered here, Namakdan on the island of Qeshm and Hormuz Island (Figs 1, 2, 3), were in a small group of near-coastal diapirs partially truncated by Holocene marine erosion at 9.3 ka (Talbot, Aftabi & Chemia, 2009). Bruthans *et al.* (2006) used the current altitudes of dated oysters and bivalves that lived close to sea level in the sediments deposited on these terraces to constrain their subsequent rates of rise at several localities in these two diapirs (Figs 2, 3). Estimating the viscosity of diapiric salt is important, as this is one of the parameters controlling (1) the growth of the diapir, and (2) entrainment of embedded dense blocks, either anhydrites or (potentially) canisters of radioactive waste (Koyi, 2001; Chemia, Koyi & Schmeling, 2008 and references therein).

The Namakdan diapir has a stem estimated to be 8 km (H) high and its major (m) and minor (n) axes have lengths 7 km and 6.8 km, respectively, in map forms and cross-sections (see Fig. 5 for our terminology). These geometric parameters for the Hormuz diapir are H = 10 km, m = 8.5 km and n = 6.8 km (Koop & Stonely, 1982; Bahroudi & Talbot, 2003; Bruthans *et al.* 2006). We note that parameter 'H' is within the usual limit of 6–10 km for most diapirs, excluding their allochthonous crests or overhangs (Dennis, 1987). The rise rates of the Hormuz and the Namakdan diapirs were much faster than the uplift rate of 0.2 mm y^{-1}

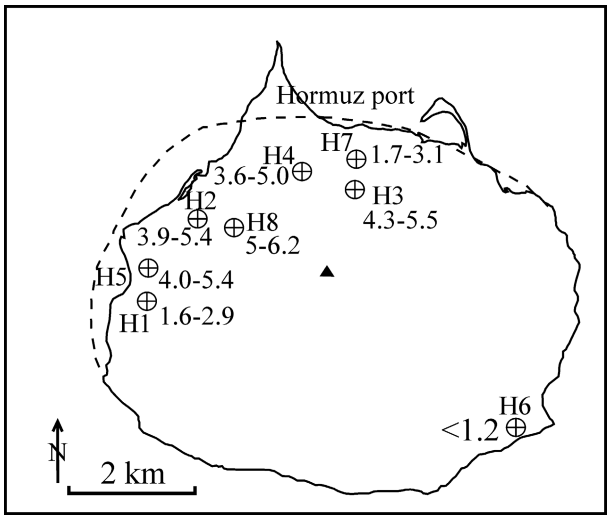

Figure 2. Extrusion rates at known locations (H1 to H8) in the Hormuz diapir. The triangle represents the centre of the diapir. Reproduced with permission from Bruthans, J. *et al.* 2006. Holocene marine terraces on two salt diapirs in the Persian Gulf, Iran: age, depositional history and uplift rates. *Journal of Quaternary Science* **21**, 843–57, Wiley-Blackwell.

for the Persian Gulf coast over the last 250 ka (Reyss *et al.* 1998). The rim of Hormuz Island rose at 2 mm y^{-1} over the last 10^4 years while the highest part of the terrace was uplifted at 5–6 mm y^{-1} (Bruthans *et al.* 2006). Seven out of the eight local rise rates constrained for the Hormuz Island salt and all the local rates on Namakdan fit well with the parabolic curves expected for the extrusion of Newtonian viscous fluids (Fig. 4) from a cylindrical channel with a central maximum of 7 ± 1 mm y^{-1} (Bruthans *et al.* 2006). Notably, this

https://doi.org/10.1017/S001675680999077X Published online by Cambridge University Press

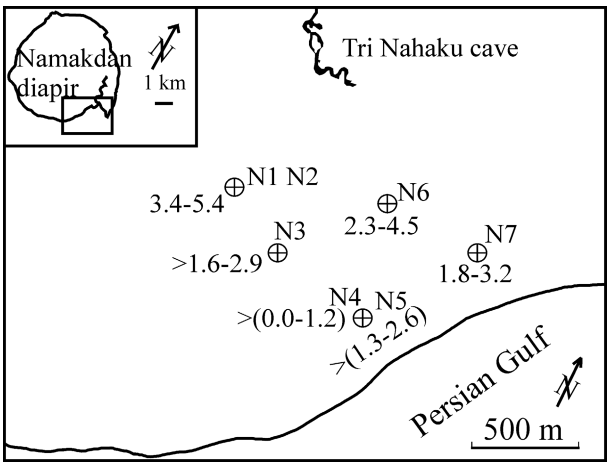

Figure 3. Extrusion rates at known locations (N1 to N7) in the Namakdan diapir. Reproduced with permission from Bruthans, J. *et al.* 2006. Holocene marine terraces on two salt diapirs in the Persian Gulf, Iran: age, depositional history and uplift rates. *Journal of Quaternary Science* **21**, 843–57, Wiley-Blackwell.

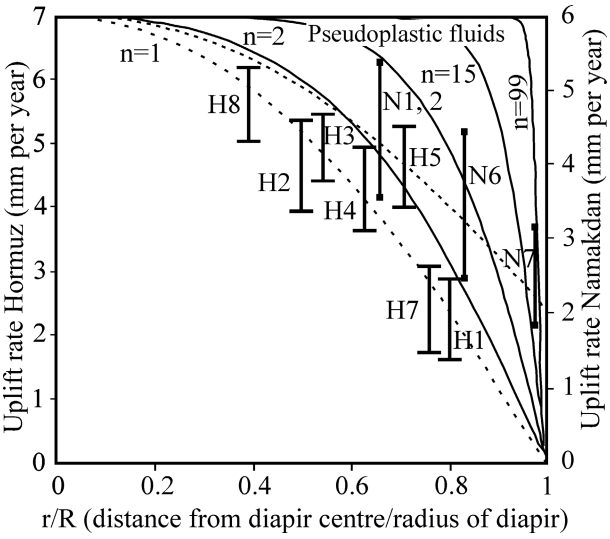

Figure 4. Uplift rates of the Hormuz and Namakdan diapirs plotted against locations. A Newtonian viscous behaviour of the salts is shown by broken lines. The zone for the pseudoplastic behaviour of the salt is at the right hand side. Reproduced with permission from Bruthans, J. *et al.* 2006. Holocene marine terraces on two salt diapirs in the Persian Gulf, Iran: age, depositional history and uplift rates. *Journal of Quaternary Science* **21**, 843–57, Wiley-Blackwell.

finding is contrary to the plug-like velocity profiles expected for non-Newtonian fluids flowing through cylindrical channels (Turcotte & Schubert, 2002). It is also contrary to the previously envisaged non-Newtonian flow of dry salt of diapirs at shallow depths (cf. Heard, 1972; Carter *et al.* 1993; Talbot & Jarvis, 1984; Jackson & Talbot, 1986; Rischbieter, 1988; Hunsche & Hampel, 1999 and references therein; Massimi *et al.* 2007; Chemia & Koyi, 2008).

Gravity spreading of the salt extruded from the diapirs of Namakdan and Hormuz Island in the last 10^4 years is unlikely, because the maximum heights reached by the extruded terraces are only 20 m and 27 m, respectively, above sea level over 1 km from the salt contacts (Bruthans *et al.* 2006) We judge these heights as too low to induce gravitational spreading. Any gravity spreading should have taken part of the salt outside the line that traces the boundary of the stem in the vertical direction (e.g. Ramberg, 1981; Talbot & Aftabi, 2004 and references therein). Most importantly, had the extruded salt undergone significant gravity spreading in the last 10^4 years, the velocity profile of extrusion should have not have matched with the parabolic profile of the Poiseuille flow of salt with Newtonian or any non-Newtonian rheology. Thus the present parabolic profiles of the Hormuz and the Namakdan diapirs indicate not only their Newtonian rheology, as already established by Bruthans *et al.* (2006), but also the fact that they have undergone insignificant gravity spreading.

Depending on the vegetation and the weathered materials that protect the diapirs from temporarily varying low rainfall in the arid setting, the (vertical) denudation rates of the Hormuz diapir vary from 20 to 50 mm y^{-1} and that of the Namakdan diapir from 7 to 50 mm y^{-1} (Bruthans *et al.* 2008, 2009). Inserting data for the extrusion rates at specific locations on these diapirs, as calculated by Bruthans *et al.* (2006), into the equations of velocity profiles deduced in this work, we constrain ranges of viscosities of these diapiric salts. We then compare our results with salt viscosities previously reported in different contexts.

2. Extrusion model of salt diapirs and their viscosity estimation

Following Bruthans *et al.* (2006), the pressure exerted by the Phanerozoic limestones (with some Palaeozoic and Cenozoic siliciclastic rocks) with a density higher than that of the subjacent Neoproterozoic–Cambrian salt is taken as the extrusion mechanism of the Hormuz and Namakdan salt diapirs (Fig. 2) (also see Mouthereau, Lacombe & Meyer, 2006; Jenyon, 1986 and references therein; Weinberger *et al.* 2006 for Mount Sedom in Dead Sea; analogue models by Talbot & Aftabi, 2004). We model parabolic profiles of these extrusions (Bruthans *et al.* 2006) as the flow of an incompressible Newtonian viscous salt through smooth-walled vertical channels with uniform cross-sections that are either elliptical or circular. The channel is comparable with the diapiric stem. For modelling purposes, we assume (1) these simple channel geometries, and (2) a single viscosity value for each of the diapirs independent of depth, and therefore of temperature. This approach is similar to that adopted by Weinberger *et al.* (2006) for the salt in the Mount Sedom salt structure beside the Dead Sea. Whereas Weinberger *et al.* (2006) considered the cross-section of the Sedom salt diapir to be a rectangle defined by parallel walls of the stem or the channel, we consider the channel to have either an elliptical (Eqs 20 and 22 in the Appendix) or circular (Eqs 23 and 24 in the Appendix) cross-section, as is the natural case

https://doi.org/10.1017/S001675680999077X Published online by Cambridge University Press

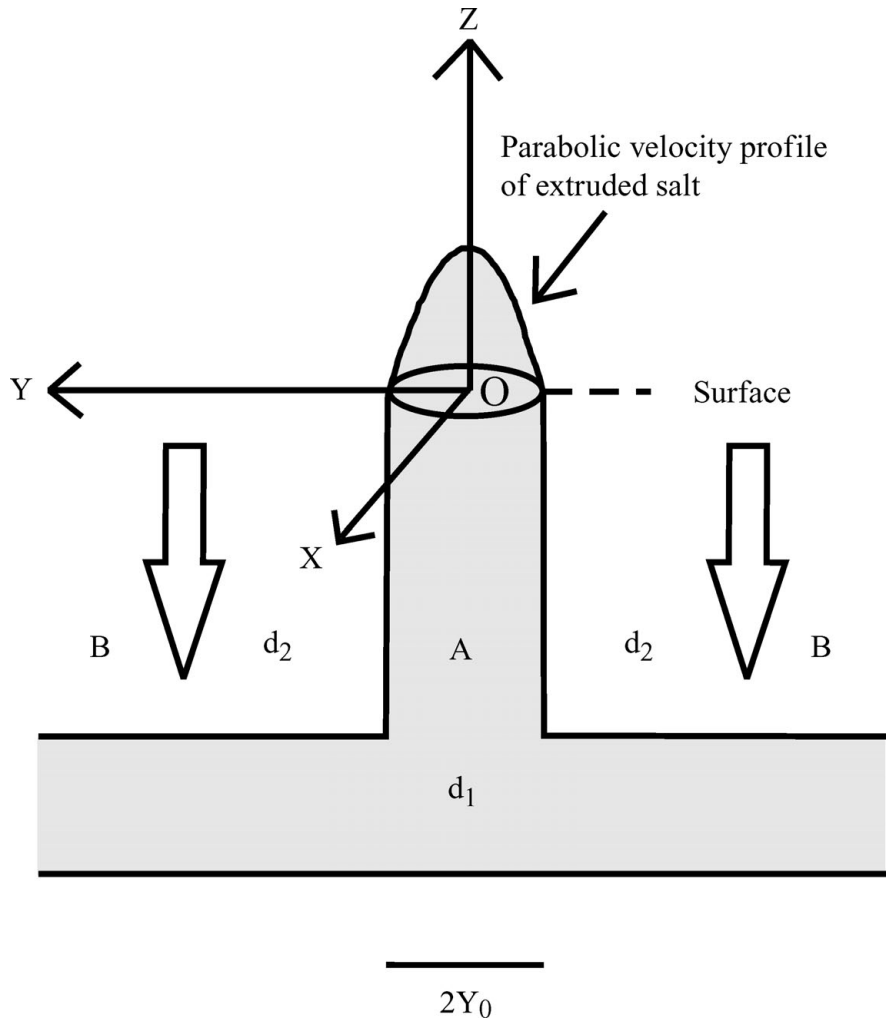

Figure 5. Our mechanical model of an extruding salt diapir in a vertical cross-section and its terminology. 'A' is a vertical channel or stem of length 'H' through the country rocks of carbonates. The cross-section of the stem 'A' for Hormuz Island is elliptical with major and minor axes of lengths '2a' and '2b' along the 'X' (east–west) and the 'Y' (north–south) axes, respectively. On the other hand, the cross-section for the Namakdan diapir is taken as circular with diameter '2a'or '2b'. In both cases 'A' is connected at the base to a horizontal channel (or source layer), and both of them are filled with an incompressible Newtonian viscous fluid with a density d_1. The horizontal channel is under compression (hollow arrows) by an overburden fluid 'B', with a density d_2 ($> d_1$). The fluid is driven upward through 'A' and extrudes into air with a velocity profile that is parabolic and distinctive of Newtonian fluids.

for the Hormuz and the Namakdan diapir, respectively. In the study case of Weinberger *et al.* (2006), the distance between the channel walls is one of the parameters that define the extrusion profile. In our case, the lengths of the major and the minor axes (Eq. 22) and the radius (Eq. 23) act as some of the few controlling parameters. In our calculation, we considered the salt as an incompressible material, following Warren (2006) and Hudec & Jackson (2007).

In our model, a deep-seated horizontal bed of salt acts as the source layer for the extruding salt. The salt rises up through a connected vertical cylindrical channel and extrudes out of a vent in the horizontal surface. Such extrusion is driven by a constant upward pressure through the vertical channel exerted by a higher density overburden onto the horizontal bed. Such simplistic models have been common, for example, in Price & Cosgrove (1990), Talbot & Aftabi (2004), Bruthans *et al.* (2006) and Weinberger *et al.* (2006), and assume salt with a constant viscosity to extrude through a vertical stem, although in a different context, thermal plumes in a mantle consisting of fluids with temperature dependent viscosities also form stems (Lin & van Keken, 2006). So far we do not have any report of flaring-upwards morphology of the Hormuz and the Namakdan diapirs, therefore it is reasonable to model their extrusion via vertical stems. In order to maintain the extrusion of salt diapirs in our case, the upward pressure that drives the extrusion has to remain higher than the temporally increasing downward pressure exerted by the emergent salt. The downward pressure exerted by the overburden on the source layer is expressed in terms of (i) the acceleration due to gravity, (ii) time elapsed since extrusion initiated, (iii) the density difference between the overburden and the salt, (iv) the length of the diapiric stem, (v) the viscosity

https://doi.org/10.1017/S001675680999077X Published online by Cambridge University Press

Table 1. Calculation of the viscosity of the Hormuz diapir

Sample number	'x' coordinate (in km)*	'y' coordinate (in km)*	Extrusion rate U_z (x,y,t) (in mm y^{-1}) in Eq. (22)†	Viscosity (μ)‡	
				For $d_{max\ diff}$ = 0.8 gm cm^{-3}: μ_{max} (in Pa s)	For $d_{min\ diff}$ = 0.17 gm cm^{-3}: μ_{min} (in Pa s)
H_3	+0.39	+1.17	5.00	1.29×10^{20} **1×10^{18}**	2.67×10^{19} 1.1×10^{18}
H_4	−0.44	+1.5	4.27	2.56×10^{20} **1×10^{18}**	5.4×10^{19} 1.04×10^{18}
H_7	+0.50	+1.89	2.50	1.74×10^{20} **1×10^{18}**	3.6×10^{19} 1.1×10^{18}
H_8	−1.5	+0.61	5.7	1.08×10^{20} **1×10^{18}**	2.2×10^{19} 1.1×10^{18}
H_2	−1.83	0.83	4.7	**8.75×10^{20}** **1×10^{18}**	1.85×10^{20} 1.03×10^{18}
H_1	−3.05	−0.47	2.2	1.52×10^{20} **1×10^{18}**	3.2×10^{20} 1.1×10^{18}
H_5	−2.83	−0.11	4.7	8.82×10^{18} **1×10^{18}**	1.8×10^{18} 1.1×10^{18}

*Calculated from figure 2 of Bruthans *et al.* (2006)
†Calculated from figure 9a of Bruthans *et al.* (2006)
‡Calculation of viscosity (μ) using Eq. (22)
Calculation of viscosity (μ) of salt of the Hormuz diapir, taking into account (1) its elliptical cross-section with the length of the major and minor axes, 'X' and 'Y', along the east–west and the north–south directions, as '2a' = 8.5 km and '2b' = 6 km, respectively (Bruthans *et al.* 2006); (2) the rate of salt extrusion $U_z(x,y,t)$; (3) the respective coordinates (x,y); and (4) the maximum ($d_{max\ diff}$ = 0.8 gm cm^{-3}) and the minimum ($d_{min\ diff}$ = 0.17 gm cm^{-3}) density differences between the salt and the surrounding limestone. Eq. (22) is used to calculate 'μ'. The parameters $U_z(x,y,t)$ and (x,y) are obtained from figures 2 and 9a, respectively, of Bruthans *et al.* (2006). Out of 28 calculated viscosity values, the maximum and the minimum values (8.75×10^{20} Pa s ∼ 10^{21} Pa s and 10^{18} Pa s) are shown in bold.

of the salt, and (vi) the major and the minor axes of the elliptical cross-section (Eq. 21 in the Appendix). The extrusion rate at any point in the elliptical cross-section is additionally dependent on (vii) the coordinate of that point (Eq. 22 in the Appendix). For a circular cross-section, the aforementioned parameters (vi) and (vii) are substituted by (vi′) the radius of the cross-section, and (vii′′) the distance of the location of known extrusion rate from the centre (Eq. 23 in the Appendix).

These derivations are based on the following constraints: (1) The source layer of salt is originally horizontal. In reality, however, it could have been folded and faulted. (2) The extruded salt does not undergo gravitational spreading, as documented by field studies (Bruthans *et al.* 2009). In other words, the extruded salt rises but does not flow laterally into an overhang. This means that the weight of the extruded salt acts downward only on the stem. (3) Erosion/dissolution of the diapiric salt is neglected. (4) The denser overburden that drove the extrusion of the diapir is taken solely to be limestone. The presence of other less dense rocks might have reduced the density, thereby leading to a range of possible density values of the overburden. The maximum and minimum possible differences in densities between the salt and the carbonate country rocks, $d_{max\ diff}$ and $d_{min\ diff}$, are taken from Mizutani (1984). The uplift rates, $U_z(x,y,t)$ and $U_z(y_1,t)$, used to calculate viscosities in this work are obtained from the seven data points for the Hormuz and the six data points for the Namakdan diapir, from figures 9a and b of Bruthans *et al.* (2006). An alternative and more accurate (but less tractable) way of constraining the viscosity of the diapiric salts could be to consider the three-dimensional Poiseuille flow for the range of viscosities by matching the best fit paraboloid of revolution obtained from Bruthans *et al.*'s (2006) data.

The viscosity (μ) of the salt of the Hormuz diapir is estimated from Eq. 22 in the Appendix which considers the diapiric cross-section to be elliptical (Table 1). The centre of the ellipse through which its major and minor axes pass is given in figure 9a of Bruthans *et al.* (2006). The coordinate axes, X and Y, chosen in this work are coincident with the W–E major and the N–S minor axes of the cross-section. The east and the north directions are taken as positive. The seven locations on this cross-section where Bruthans *et al.* (2006) obtained uplift rates are converted into (x,y) coordinates in Table 1. Negative values of some of the 'x' (or 'y') coordinates indicate that those points are west (or south) of the centre of the diapir.

In their figure 9b, Bruthans *et al.* (2006) did not show the centre of the Namakdan diapir. This prevented locating the coordinate axes on its cross-section, transforming locations of known uplift rates into coordinates, and in effect, estimating the viscosity considering the more precise geometry of the cross-section. However, Bruthans *et al.* (2006, fig. 10) did locate uplift rates from the centre. Alternately, therefore, the viscosity of the Namakdan diapir is estimated (Table 2) taking its cross-section to be circular, using Eq. 23 in the Appendix. In this calculation, the equation requires only the distances of

https://doi.org/10.1017/S001675680999077X Published online by Cambridge University Press

Table 2. Calculation of the viscosity of the Namakdan diapir

Sample number*	Distance from salt diapir centre (m); 'y_1' in Eq. (23)*	Extrusion rate (mm y^{-1}); 'U_z (y_1,t)' in Eq. (23)*	Salt viscosity (μ) for $2y_0 = 7$ km†		Salt viscosity (μ) or $2y_0 = 6.8$ km†	
			For $d_{max\ diff}$ = 0.8 gm cm^{-3}	For $d_{min\ diff}$ = 0.17 gm cm^{-3}	For $d_{max\ diff}$ = 0.8 gm cm^{-3}	For $d_{min\ diff}$ = 0.17 gm cm^{-3}
			μ_{max} (in Pa s)	μ_{min} (in Pa s)	μ_{max} (in Pa s)	μ_{min} (in Pa s)
$N_{1/2}$	2250	4.7	8.9×10^{19}	1.99×10^{20}	7.39×10^{19}	1.67×10^{20}
			1.2×10^{18}	1.5×10^{18}	$\mathbf{1.15\times10^{17}}$	3.3×10^{19}
$N_{2/1}$	2250	4.1	1.09×10^{20}	2.1×10^{19}	1.9×10^{20}	1.97×10^{19}
			1.2×10^{18}	1.4×10^{18}	3.8×10^{19}	1.7×10^{18}
N_{7a}	3310	2.55	3.1×10^{19}	$\mathbf{6.5\times10^{20}}$	1.38×10^{20}	No real solution
			1.2×10^{18}	2.95×10^{18}	1.2×10^{18}	
N_{7b}	3310	2.45	3.1×10^{19}	5.3×10^{18}	1.38×10^{20}	No real solution
			1.2×10^{18}	8.6×10^{17}	1.2×10^{18}	
N_{6d}	2800	3.75	6.03×10^{18}	1.66×10^{19}	5.89×10^{20}	1.16×10^{19}
			1.5×10^{18}	1.4×10^{18}	1.15×10^{18}	1.18×10^{18}
N_{6x}	2800	3.0	7.6×10^{18}	1.86×10^{19}	7.39×10^{19}	1.67×10^{19}
			1.4×10^{18}	1.4×10^{18}	1.15×10^{18}	3.15×10^{17}

*From figure 9b of Bruthans *et al.* (2006); †salt viscosity (μ) calculated using Eq. (23).
Calculation of viscosity (μ) of salt of the Namakdan diapir considering (1) its sub-circular cross-section as circular and taking the major (7 km) and minor axes (6.8 km) as diameters in two sets of calculations; (2) the 'y_1' values as obtained from figure 9b of Bruthans *et al.* (2006), these are presented here in a column; and (3) the density values, $d_{max\ diff}$ and $d_{min\ diff}$, as per caption of Table 1. Eq. (23) is used to calculate 'μ'. The maximum and the minimum of 44 calculated viscosities (6.5×10^{20} Pa s $\sim10^{21}$ Pa s and 1.15×10^{17} Pa s $\sim10^{17}$ Pa s), are shown in bold in the table.

sample locations from the centre (the 'y_1' parameters) and not the location of the centre. We note that the cross-section is actually sub-circular with a very low ellipticity $e = m\,n^{-1} = 1.03$ ($m = 7$ km and $n = 6.8$ km: Bruthans *et al.* 2006). This indicates that the viscosity calculated assuming a circular cross-section tentatively holds good for the elliptical geometry.

3. Results and conclusions

The equations of velocity profiles involve the previously mentioned (Section 2) parameters (i) to (vii) for the elliptical cross-section (Eq. 22) of the Hormuz diapir, and (i) to (v) and (vi′) and (vii′′) for the circular cross-section of the Namakdan diapir (Eq. 23). These profiles are the quadratic equations of salt viscosity. Therefore, for a single set of these parameters at each sample point, two possible values of viscosities can be obtained. In total, the maximum and minimum values of density difference between the salt and the limestone for the Hormuz diapir give rise to four probable values bracketing ranges of salt viscosity (Table 1). In the case of the Namakdan diapir, the viscosity of the salt is estimated additionally using the two possible values of the radius of the cross-section, thus giving rise to a total of eight possible values for viscosities at each sample point (Table 2). We chose a range in densities for the salt and limestone from the literature because (1) their absolute values for the diapirs in the Persian Gulf are not available, and (2) their values may be affected by 'small proportions of impurities' (cf. Bruthans *et al.* 2008) and/or extraneous rock fragments (Kent, 1958). Thus, the variation in our list of calculated viscosities arises intrinsically from Eqs (22) and (23) in the Appendix and from the rather wide range of parameters inserted into these equations. Our model results are not meant to represent any spatial variation of viscosity within either diapir, but instead show the possible variation in estimates of a single representative value. We also note that rock salts may deform maintaining a power-law rheology on scales smaller than kilometres (e.g. Critescu & Hunsche, 1998). However, our estimation took no account of power-law rheology. Our treatment here has been essentially the first order approach of assigning a single viscosity to the whole salt sequence based on the simple parabolic extrusion profiles deduced for both diapirs by Bruthans *et al.* (2006). This is a common practice in the literature of salt tectonics, especially in analogue modelling and numerical modelling (e.g. Talbot & Jarvis, 1984; Poliakov *et al.* 1996; Talbot *et al.* 2000; Schultz-Ela & Walsh, 2002; Talbot, 2002; Schultz-Ela, 2003; Mouthereau, Lacombe & Meyer, 2006; Chemia & Koyi, 2008).

The dynamic viscosity of the salt in the Hormuz diapir lies in the range of 10^{18}–10^{21} Pa s considering its extrusion through an elliptical cross-section (Table 1; no. 38 of Table 3). The viscosity of the salt in the Namakdan diapir has been estimated by considering its sub-circular cross-section as circular. The calculated range of viscosity is 10^{17}–10^{21} Pa s (Table 2; no. 39 of Table 3).

A concise review of viscosity of salts is made in Table 3 in numbers 1 to 37. We excluded viscosity values of salts in a bi-viscous medium as given by Zulauf *et al.* (2008). The range of viscosities calculated for the salts of the Hormuz and Namakdan diapirs broadly matches earlier values reported for flowing salt (Table 3, no. 32). The estimated ranges are broader than that for Newtonian salts (Table 3, no. 19), higher than that for the average value of salt (Table 3, no. 21) and also that for salts at room temperature (Table 3, no. 26). On the other hand, the deduced ranges match with the viscosity values for other salt diapirs (Table 3, nos 3,

https://doi.org/10.1017/S001675680999077X Published online by Cambridge University Press

Table 3. A review of salt viscosities

No.	Viscosity (in Pa s)	Context	Author(s)
1	2.7×10^{10} – 4×10^{17}	Review of different salts	Odé (1968)
2	10^{19}–10^{21}	Polycrystalline halites; at stresses within the range 1–40 bar, strain rates within 10^{-4} – 10^{-16}, and temperatures within 50–200°C	Woidt (1978)
3	3×10^{17}	Salt in salt diapir, (North) Germany	Woidt (1978)
4	Viscosity of salts in subsurface unlikely to be much greater than 10^{16} Pa s		Chapman (1981)
5	2.6×10^{17}	Salts in Iranian salt diapirs	Talbot & Jarvis (1984) and references therein
6	10^{16}	Salts with non-Newtonian rheology	Jackson & Talbot (1986) and references therein
7	10^{14}–10^{20}	Dry rock salts	Jackson & Talbot (1986) and references therein
8	2.2×10^{16}	Monomineralic salts	Jackson & Talbot (1986) and references therein
9	10^{15}–10^{20}	Dry rock salt	Jackson & Talbot (1989)
10	10^{13}–10^{16}	Salts in Gulf of Mexico, the value depends on moisture and temperature	Warren (1989, 2006)
11	10^{15}–10^{20}	Salts in salt diapirs	Koyi (1991*a*) and references therein
12	5×10^{17}	Salts with mean grain size 5 mm, at 20°C	Vendeville & Jackson (1992)
13	3×10^{16}	Salts with mean grain size 5 mm, at 140°C	Vendeville & Jackson (1992)
14	$\geq 10^{19}$	Salts in salt diapirs, required for viscous stress in salt to compete with the overburden strength	Vendeville & Jackson (1992)
15	2×10^{16}	Salt at 125°C	Carter *et al.* (1993)
16	10^{15}–10^{19}	Salt at subsurface	Davison *et al.* (1993) and reference therein
17	10^{17}	Salt with small grain size and high temperature	van Keken *et al.* (1993)
18	10^{20}	Salt with large grain size and low temperature	van Keken *et al.* (1993)
19	10^{17}–10^{18}	Salts with Newtonian rheology	Weinberg (1993)
20	10^{17}–10^{19}	Salts, depending on the grain size and the water content	Jackson, Vendeville & Schultz-Ela (1994)
21	10^{16}	Average value for salts	Davis & Reynolds (1996)
22	10^{17}	Salt in numerical models	Poliakov *et al.* (1996)
23	10^{16}–10^{17}	Salts in Kuh-e-Jahani	Talbot *et al.* (2000)
24	10^{16} –10^{18}	Evaporites	Withjack & Callaway (2000)
25	10^{16}–10^{19}	Rock salt at different geologic conditions and material properties	Withjack & Callaway (2000)
26	3.5×10^{15}–4×10^{17}	Salt at room temperature	Billings (2001)
27	10^{16}–10^{17}	Salts in the Zagros Mountains	Talbot (2002)
28	10^{17}–10^{18}	Salts in salt diapirs, Persian Gulf	McQuarrie (2004)
29	10^{18}	Salt in numerical models	Gemmer *et al.* (2004); Gemmer, Beaumont & Ings (2005)
30	10^{15}	Salt at 5 km depth	Mouthereau, Lacombe & Meyer (2006)
31	10^{18}	Salts in analogue models	Schultz-Ela & Walsh (2002), Schultz-Ela (2003), Mouthereau, Lacombe & Meyer (2006)
32	10^{16}–10^{20}	Naturally flowing salts	Z. Schlèder, unpub. Ph.D. thesis, Aachen University of Technology (2006)
33	10^{17}–10^{18}	Salts in salt diapirs, Nova Scotia	Ings & Shimeld (2006)
34	2–3×10^{18}	Salts in Mt. Sedom, Dead Sea Basin	Weinberger *et al.* (2006)
35	10^{18}	Dry halite	Warren (2006)
36	10^{17}–10^{19}	Salts in numerical models	Chemia, Koyi & Schmeling (2008)
37	2.3×10^{16} – $\sim10^{23}$	Salts in numerical models	Chemia, Schmeling & Koyi (2009)
38	10^{18}–10^{21}	Salt of Hormuz diapir; considered incompressible Newtonian and extruding through elliptical cross-section (see Table 1 for details)	(this work)
39	10^{17}–10^{21}	Salt of Namakdan diapir; considered incompressible Newtonian and extruding through circular cross-section (see Table 2 for details)	(this work)

Thirty-seven values of salt viscosities presented by other authors after they surveyed the literature are tabulated in rows 1–37. The ranges of viscosities for the Hormuz and Namakdan diapirs calculated in this work are presented in rows 38 and 39.

5, 11, 27 and 33), though not with all of them (Table 3, no. 10). Further, matches with some of the previously estimated viscosities (Table 3, nos 2, 17, 18 and 20) suggest that the salt in these diapirs might have a broad range in grain-size. Interestingly, while the reported grain sizes of Hormuz salts range from > 10 mm up to 15 mm or even 4 cm, those in the Namakdan diapir vary from 3 to 8 mm (Bruthans *et al.* 2008, table 3;

https://doi.org/10.1017/S001675680999077X Published online by Cambridge University Press

Talbot, Aftabi & Chemia, 2009). This crudely matches with the predicted wide range of grain sizes of salts. The estimated range of viscosities of these two diapirs can be useful in their tectonic modelling.

Acknowledgements. SM acknowledges a 2005–2006 'Guest Scholarship' at Uppsala University from the Swedish Institute to initiate this work and a 'Seed Grant' (Spons/GS/SM-1/2009) from the Indian Institute of Technology Bombay to finish the work. HAK was supported by the Swedish Research Council. Conscientious criticism by Jiri Mls (Charles University) of an earlier version and two anonymous reviewers of Geological Magazine led us to clarify the model further. Jiri Bruthans (Charles University) updated us about salt diapirs in the Persian Gulf.

References

BAHROUDI, A. & TALBOT, C. J. 2003. The configuration of the basement beneath the Zagros basin. *Journal of Petroleum Geology* **26**, 257–82.

BILLINGS, M. P. 2001. *Structural Geology*, 3rd ed. New Delhi: Prentice Hall of India.

BOSÁK, P., JAROS, J., SPUDIL, J., SULOVSKY, P. & VACLAVAK, V. 1998. Salt plugs in the eastern Zagros, Iran: regional geological reconnaissance. *GeoLines (Praha)* **7**, 3–174.

BRUTHANS, J., ASADI, N., FILIPPI, M., VILHELM, Z. & ZARE, M. 2008. A study of erosion rates on salt diapir surfaces in the Zagros Mountains, SE Iran. *Environmental Geology* **53**, 1079–89.

BRUTHANS, J., FILIPPI, M., ASADI, N., ZARE, M. & CHURÁČKOVÁ, Z. 2009. Surficial deposits on salt diapirs (Zagros Mountains and Persian Gulf Platform, Iran): Characterization, evolution, erosion and the influence on landscape morphology. *Geomorphology* **107**, 195–209.

BRUTHANS, J., FILIPPI, M., GERŠL, M., ZARE, M., MELKOVÁ, J., PAZDUR, A. & BOSÁK, P. 2006. Holocene marine terraces on two salt diapirs in the Persian Gulf, Iran: age, depositional history and uplift rates. *Journal of Quaternary Science* **21**, 843–57.

CARTER, N. L, HORSEMAN, S. T., RUSSELL, J. E. & HANDIN, J. 1993. Rheology of rocksalt. *Journal of Structural Geology* **15**, 1257–71.

CHAPMAN, R. E. 1981. *Geology and Water, An Introduction to Fluid Mechanics for Geologists. Volume 1*. The Hague: Martinus Nijhoff, 183 pp.

CHEMIA, Z. & KOYI, H. A. 2008. The control of salt supply on entrainment of an anhydrite layer within a salt diapir. *Journal of Structural Geology* **30**, 1192–1200.

CHEMIA, Z., KOYI, H. A. & SCHMELING, H. 2008. Numerical modeling of rise and fall of a dense layer in salt diapirs. *Geophysical Journal International* **172**, 798–816.

CHEMIA, Z., SCHMELING, H. & KOYI, H. 2009. The effect of salt viscosity on future evolution of the Gorleben salt diapir, Germany. *Tectonophysics* **473**, 446–56. DOI: 10.1016/j.tecto.2009.03.027.

CRITESCU, N. D. & HUNSCHE, U. 1998. *Time effects in Rock mechanics. Series: Materials, modelling and Computation*. Chichester: John Wiley and Sons, 342 pp.

DAVIES, G. F. 1999. *Dynamic Earth, Plumes and Mantle Convection*. Cambridge University Press, 263 pp.

DAVIS, G. H. & REYNOLDS, S. J. 1996. *Structural Geology of Rocks and Regions*, 2nd edn. New York: John Wiley, 652 pp.

DAVISON, I., INSLEY, M., HARPER, M., WESTON, P., BLUNDELL, D., MCCLAY, K. & QUALLINGTON, A. 1993. Physical modeling of overburden deformation around salt diapirs. *Tectonophysics* **228**, 255–74.

DE BÖCKH, H., LEES, G. M. & RICHARDSON, F. D. S. 1929. Contribution to the stratigraphy and tectonics of the Iranian ranges. In *The structure of Asia* (ed. J. W. Gregory), pp. 58–176. London: Methuen.

DENNIS, J. G. 1987. *Structural Geology: An Introduction*. Dubuque: Wm. C. Brown Publishers, 464 pp.

GEMMER, L., BEAUMONT, C. & INGS, S. J. 2005. Dynamic modelling of passive margin salt tectonics: effects of water loading, sediment properties and sedimentation. *Basin Research* **17**, 383–402.

GEMMER, L., INGS, S. J., MEDVEDEV, S. & BEAUMONT, C. 2004. Salt tectonics driven by differential sediment loading: stability analysis and finite element experiments. *Basin Research* **16**, 199–218.

HARRISON, J. V. 1930. The geology of some salt-plugs in Laristan, southern Persia. *Quarterly Journal of the Geological Society of London* **86**, 463–522.

HARRISON, G. V. 1931. Salt Domes in Persia. *Journal of Institution of Petroleum Technology* **17**, 300–20.

HEARD, H. C. 1972. Steady-state flow in polycrystalline halite at pressure of 2 kilobars. In *Flow and Fracture of Rocks* (eds H. C. Heard, I. Y. Borg, N. L. Carter & C. B. Raleigh), pp. 191–209. Griggs Volume. American Geophysical Union Monograph no. 16.

HUDEC, M. R. & JACKSON, M. P. A. 2007. Terra Infirma: Understanding Salt Tectonics. *Earth-Science Reviews* **82**, 1–28.

HUNSCHE, U. & HAMPEL, A. 1999. Rock salt-mechanical properties of the host rock material for a radioactive waste repository. *Engineering Geology* **52**, 271–91.

INGS, S. J. & SHIMELD, J. W. 2006. A new conceptual model for the structural evbolution of a regional salt detachment on the northern Scotian margin, offshore eastern Canada. *AAPG Bulletin* **90**, 1407–23.

JACKSON, M. P. A. & TALBOT, C. J. 1986. External shapes, strain rates and dynamics of salt structures. *Geological Society of America Bulletin* **97**, 305–25.

JACKSON, M. P. A. & TALBOT, C. J. 1989. Anatomy of mashroom-shaped diapirs. *Journal of Structural Geology* **11**, 211–30.

JACKSON, M. P. A., VENDEVILLE, B. C. & SCHULTZ-ELA, D. D. 1994. Structural Dynamics of Salt Systems. *Annual Review of Earth and Planetary Sciences* **22**, 93–117.

JAHANI, S., CALLOT, J. P., DE LAMOTTE, D. F., LETOUZEY, J. & LETURMY, P. 2007. The Salt Diapirs of the Eastern Fars Province (Zagros, Iran): A Brief Outline of their Past and Present. In *Thrust Belts and Foreland Basins from Fold Kinematics to Hydrocarbon Systems* (eds O. Lacombe, J. Lavé, F. Roure & J. Vergés), pp. 289–308. Springer Verlag.

JENYON, M. K. 1986. *Salt Tectonics*. London: Elsevier Applied Science Publishers, 192 pp.

KENT, P. E. 1958. Recent studies of South Persian salt plugs. *American Association of Petroleum Geologists Bulletin* **42**, 2951–79.

KOOP, W. J. & STONELY, R. 1982. Subsidence history of the Middle East Zagros basin, Permian to recent. In *Philosophical Transactions of the Royal Society, London* **A305**, 149–68.

KOYI, H. 1991*a*. Mushroom diapirs penetrating overburdens with high effective viscosities. *Geology* **19**, 1229–32.

KOYI, H. A. 1991*b*. Gravity overturn, extension and basement fault activation. *Journal of Petroleum Geology* **14**, 117–42.

KOYI, H. A. 1997. Analogue modelling: from a qualitative to a quantitative technique, a historical outline. *Journal of Petroleum Geology* **20**, 223–38.

KOYI, H. A. 2001. Modelling the influence of sinking anhydrite blocks on salt diapirs targeted for hazardous waste disposal. *Geology* **29**, 387–90.

KOYI, H. A., GHASSEMI, A., HESSAMI, KH. & DIETL, C. 2008. Modelling the role of strike-slip faults in triggering Salt Diapirs in the Zagros fold-thrust belt. *Journal of the Geological Society, London* **165**, 1031–44.

KOYI, H. A., JENYON, M. K. & PETERSEN, K. 1993. The effect of basement faulting on diapirism. *Journal of Petroleum Geology* **16**, 285–312.

LIN, S.-C. & VAN KEKEN, P. E. 2006. Dynamics of thermo-chemical plumes: 1. Plume formation and entrainment of a dense layer. *Geochemistry, Geophysics, Geosystems* **7**, Q02006. DOI:10.1029/2005GC001071.

MASSIMI, P., QUARTERONI, A., SALERI, F. & SCROFANY, G. 2007. Modelling of salt tectonics. *Computational Methods in Applied Mechanics and Engineering* **197**, 281–93.

MCQUARRIE, N. 2004. Crustal scale geometry of the Zagros fold-thrust belt, Iran. *Journal of Structural Geology* **26**, 519–35.

MIZUTANI, S. 1984. Salt Domes in the Gulf Coast. In *Geological Structures* (eds T. Uemura & M. Mizutani), pp. 106–33. Chichester: John Wiley & Sons.

MOUTHEREAU, F., LACOMBE, O. & MEYER, B. 2006. The Zagros folded belt (Fars, Iran): constraints from topography and critical wedge modeling. *Geophysical Journal International* **165**, 336–56.

ODÉ, H. 1968. Review of Mechanical Properties of Salt Relating to Salt-Dome Genesis. In *Diapirism and Diapirs* (eds J. Braunstein & G. D. O'Brien), pp. 53–8. 50th Annual Meeting of the Association in New Orleans, Louisiana, April 26–29, 1965. Memoir 8. The American Association of Petroleum Geology.

PAPANASTASIOU, C. T., GEORGIOU, G. C. & ALEXANDROU, A. N. 2000. *Viscous Fuid Flow*. Florida: CRC Press, 253 pp.

POLIAKOV, A. B., PODLADCHIKOV, YU. YU., DAWSON, E. CH. & TALBOT, C. J. 1996. Salt diapirism with simultaneous brittle faulting and viscous flow. In *Salt Tectonics* (eds G. I. Alsop, D. J. Blundell & I. Davison), pp. 291–302. Geological Society of London, Special Publication no. 100.

PRICE, N. J. & COSGROVE, J. W. 1990. *Analysis of Geological Structures*. Cambridge University Press, 520 pp.

RAMBERG, H. 1981. *Gravity, deformation and the Earth's crust in theory, experiments and geological applications*, 2nd ed. London: Academic Press.

REYSS, J. L., PIRAZZOLI, P. A., HAGHIPOR, A., HATTE, C. & FONTUGNE, M. 1998. Quaternary marine terraces and tectonic uplift rates in the south coast of Iran. In *Coastal tectonics* (eds I. S. Stewart & C. Vita-Finzi), pp. 225–37. Geological Society of London, Special Publication no. 146.

RISCHBIETER, F. 1988. Stress distribution and flow field in salt domes. Proceedings of the Second Conference. In *The Mechanical Behaviour of Salt* (eds H. R. Hardy & M. Langer), pp. 615–24. Federal Institute for Geosciences and National Resources, Hanover, September 24–28, 1984. Clausthal-Zellerfeld: Trans Tech Publication.

SANS, M. & KOYI, H. A. 2001. Modelling the role of erosion in diapir development in contractional settings. In *Tectonic Modelling: A Volume in Honor of Hans Ramberg* (eds H. A. Koyi & N. Mancktelow), pp. 111–22. Geological Society of America, Memoir no. 193.

SCHUBERT, G., TURCOTTE, D. L. & OLSON, P. 2001. *Mantle Convection in the Earth and Planets. Part I*. Cambridge University Press, 498 pp.

SCHULTZ-ELA, D. D. 2003. Origin of drag folds bordering salt diapirs. *AAPG Bulletin* **87**, 757–80.

SCHULTZ-ELA, D. D. & WALSH, P. 2002. Modeling of grabens extending above evaporites in Canyonlands National Park, Utah. *Journal of Structural Geology* **24**, 247–75.

TALBOT, C. J. 1998. Extrusions of Hormoz salt in Iran. In *Lyell: the Past is the Key to the Present* (eds D. J. Blundell & A. C. Scott), pp. 315–34. Geological Society of London, Special Publication no. 143.

TALBOT, C. J. 2002. Salt extrusion-rates in the Zagros. In *Basic and Applied Salt Mechanics* (eds N. D. Cristescu, H. R. Hardy & R. O. Simionescu), pp. 35–9. Proceedings of the Fifth Conference on Mechanical Behaviour of Salt, Mecasalt V, Bucharest, Romania, 9–11 August 1999. A. A. Balkema Publishers.

TALBOT, C. J. & AFTABI, P. 2004. Geology and models of salt extrusion at Qum Kuh, central Iran. *Journal of the Geological Society, London* **161**, 321–34.

TALBOT, C. J. & AFTABI, P. & CHEMIA, Z. 2009. Potash in a salt mushroom at Hormoz island, Hormoz strait, Iran. *Ore Geology Reviews* **35**, 317–32.

TALBOT, C. J., FARHADI, R. & AFTABI, P. 2009. Potash in salt extruded at Sar Pohl diapir, southern Iran. *Ore Geology Reviews* **35**, 352–6.

TALBOT, C. J. & JARVIS, R. J. 1984. Age, budget and dynamics of an active salt extrusion in Iran. *Journal of Structural Geology* **6**, 521–33.

TALBOT, C. J., MEDVEDEV, S., ALAVI, M., SHAHRIVAR, H. & HEIDARI, E. 2000. Salt extrusion rates at Kuh-e-Jahani, Iran: June 1994 to November 1997. In *Lyell: the Past is the Key to the Present* (eds D. J. Blundell & A. C. Scott), pp. 93–110. Geological Society of London, Special Publication no. 143.

TURCOTTE, D. L. & SCHUBERT, G. 2002. *Geodynamics*, 2nd ed. Cambridge University Press.

VAN KEKEN, P. E., SPIERS, C. J., VAN DEN BERG, A. P. & MUYZERT, E. J. 1993. The effective viscosity of rock salt: implementation of steady-state creep laws in numerical models of salt diapirism. *Tectonophysics* **225**, 457–76.

VENDEVILLE, B. C. & JACKSON, M. P. A. 1992. The rise of diapirs during thin-skinned extension. *Marine Petroleum Geology* **9**, 331–54.

WARREN, J. K. 1989. *Evaporite Sedimentology: Importance in Hydrocarbon Accumulation*. Prentice Hall, 320 pp.

WARREN, J. K. 2006. *Evaporites: Sediments, Resources and Hydrocarbons*. Berlin: Springer, 1036 pp.

WEINBERG, R. F. 1993. The upwelling transport of inclusions in Newtonian and power-law salt diapirs. *Tectonophysics* **228**, 141–50.

WEINBERGER, R., LYAKHOVSKY, V., BAER, G. & BEGIN, Z. B. 2006. Mechanical modeling and InSAR measurements of Mount Sedom uplift, Dead Sea basin: Implications for effective viscosity of rock salt. *Geophysics Geochemistry Geosystems* **7**, Q05014, DOI: 10.1029/2005GC001185.

WEIJERMARS, R., JACKSON, M. P. A. & VENDEVILLE, B. 1993. Rheological and tectonic modeling of salt provinces. *Tectonophysics* **217**, 143–74.

WITHJACK, M. O. & CALLAWAY, S. 2000. Active Normal Faulting Beneath a Salt Layer: An Experimental Study of Deformation Patterns in the Cover Sequence. *AAPG Bulletin* **84**, 627–51.

WOIDT, W.-D. 1978. Finite element calculations applied to salt dome analysis. *Tectonophysics* **50**, 369–86.

ZULAUF, G., ZULAUF, J., BORNEMANN, O., KIHM, N., PEINL, M. & ZANELLA, F. 2008. Experimental deformation of a single-layer anhydrite in halite matrix under bulk constriction. Part 1. Geometric and kinematic aspects. *Journal of Structural Geology* **31**, 460–74.

Appendix.

The Poisson equation of rectilinear flow of an incompressible Newtonian viscous fluid in the Z-direction, in an infinitely long parallel-wall inclined channel, is given by:

$$(\partial^2 U_z/\partial x^2) + (\partial^2 U_z/\partial y^2) = \mu^{-1}[(\partial P/\partial x) - d_1\, g\, \mathrm{Sin}\theta] \quad (1)$$

Eq. (1) is the same as equation 6.190 of Papanastasiou, Georgiou & Alexandrou (2000) but with our choice of symbols (see Fig. 5). Here 'X' and 'Y' are the mutually perpendicular axes, both of which are perpendicular to the 'Z' direction. 'X' and 'Y' lie on the cross-section of the channel. 'U_z': velocity of the fluid in the Z-direction. μ: dynamic viscosity of the fluid. $(\partial P/\partial x)$: pressure gradient in the fluid along the X-direction. d_1: density of the fluid. g: acceleration due to gravity. θ: inclination of the channel.

Referring to Figure 5, we now consider that (1) the channel is very long so as to develop a channel flow but of finite length (= 10 km and 8 km for the two diapirs); (2) the channel is vertical; (3) the fluid rises up the channel due to pressure exerted by the surrounding overburden of higher density on the horizontal source layer; and (4) the cross-section of the channel is elliptical with 'X' and 'Y' as the major and the minor axes with lengths '2a' and '2b', respectively. From constraint (2), $d_1\, g\, \mathrm{Sin}\theta = d_1\, g$. Applying this and constraint (3), $(\partial P/\partial x) = [d_2\, g - P_{out}(t)\, H^{-1}]$, where $P_{out}(t)$ stands for the pressure exerted by the extruded fluid. Therefore, the resultant pressure gradient acting vertically upward on the fluid channel 'A' at depth H, that is, the expression $[(\partial P/\partial x) - d_1\, g\, \mathrm{Sin}\theta]$ in Eq. (1), is equal to $[g\,(d_2 - d_1) - P_{out}(t)\, H^{-1}]$. Thus, Eq. (1) becomes

$$(\partial^2 U_z/\partial x^2) + (\partial^2 U_z/\partial y^2) = \mu^{-1}[g(d_2 - d_1) - P_{out}(t)\, H^{-1}] \quad (2)$$

Let $U_z(x,y,t)$ be the velocity of the extruding fluid at co-ordinate (x,y) at an instant in time 't'. Considering the channel walls to be static during the fluid flow, the boundary condition is $U_z(x,y,t) = 0$ at

$$(x^2\, a^{-2} + y^2\, b^{-2}) = 1 \quad (3)$$

A dependent variable U'_z is introduced such that

$$U_z(x,y,t) = U'_z(x,y,t) + c_1\, x^2 + c_2\, y^2 \quad (4)$$

Here 'c_1' and 'c_2' are non-zero constants and are to be solved so that: (1) $U'_z(x,y,t)$ satisfies the Laplace equation, and (2) $U'_z(x,y,t)$ is constant on the wall at a particular instant 't'. Substituting Eq. (4) into Eq. (2),

$$(\partial^2 U_z/\partial x^2) + (\partial^2 U'_z/\partial y^2) + 2(c_1 + c_2) = \mu^{-1}[(d_2 - d_1)g - P_{out}(t)H^{-1}] \quad (5)$$

$U'_z(x)$ will satisfy the Laplace Equation:

$$(\partial^2 U'_z/\partial x^2) + (\partial^2 U'_z/\partial y^2) = 0 \quad (6)$$

if

$$2(c_1 + c_2) = \mu^{-1}[(d_2 - d_1)\, g - P_{out}(t)\, H^{-1}] \quad (7)$$

From the boundary condition (Eq. 3),

$$U'_z x,y,t = -(c_1\, x^2 + c_2\, y^2) = -c_1(x^2 + c_2\, c_1^{-1}\, y^2); \quad \text{at}\ (x^2\, a^{-2} + y^2\, b^{-2}) = 1 \quad (8)$$

Writing

$$(c_2\, c_1^{-1}) = (a^2\, b^{-2}) \quad (9)$$

$U'_z(x,y,t)$ is constant at the channel boundary at a particular instant 't':

$$U'_z(x,y,t) = -c_1\, a^2\ \text{on}\ (x^2\, a^{-2} + y^2\, b^{-2}) = 1 \quad (10)$$

According to the maximum principle for the Laplace equation, $U'_z(x,y,t)$ has both its minimum and maximum values on the boundary of the domain. This means that $U'_z(x,y,t)$ is constant over the whole domain at a particular time:

$$U'_z(x,y,t) = -c_1\, a^2 \quad (11)$$

Putting Eq. (11) into Eq. (4), and using Eq. (9):

$$U_z(x,y,t) = (-c_1\, a^2 + c_1\, x^2 + c_2\, y^2) = -c_1\, a^2(1 - x^2\, a^{-2} - c_2\, c_1^{-1}\, y^2\, a^{-2}) \quad (12)$$

or

$$U_z(x,y,t) = -c_1\, a^2(1 - x^2\, a^{-2} - y^2\, b^{-2}) \quad (13)$$

The constant 'c_1' is obtained from Eq. (7) and Eq. (9):

$$c_1 = 0.5\, b^2\, \mu^{-1}[(d_2 - d_1)\, g - P_{out}(t)\, H^{-1}]\,(a^2 + b^2)^{-1} \quad (14)$$

Putting the 'c_1' value of Eq. (14) into Eq. (13):

$$U_z(x,y,t) = -0.5\, \mu^{-1}\, a^2\, b^2[(d_2 - d_1)\, g - P_{out}(t)\, H^{-1}] \times (a^2 + b^2)^{-1}\,(1 - x^2\, a^{-2} - y^2\, b^{-2}) \quad (15)$$

Integrating the velocity profile given by Eq. (15) over the elliptical cross-section gives the volumetric flow rate:

$$Q(t) = -0.25\, \pi\, a^3\, b^3\, \mu^{-1}[(d_2 - d_1)\, g - P_{out}(t)\, H^{-1}](a^2 + b^2)^{-1} \quad (16)$$

In Eq. (16) and onwards, we assume that no part of the extruded salt flows outside the cross-section. Dividing Q(t) by the area of the elliptical cross-section ($A = \pi\, a\, b$) gives the volumetric flow rate per unit area as follows:

$$Q'(t) = Q(t)\, A^{-1} = -0.25\, a^2\, b^2\, \mu^{-1}[(d_2 - d_1)\, g - P_{out}(t)\, H^{-1}](a^2 + b^2)^{-1} \quad (17)$$

Equating $Q'(t)$ with the pressure buildup in extrusion gives

$$dP_{out}(t)/dt = Q'(t) d_1\, g = -0.25\, a^2\, b^2\, d_1\, g\, \mu^{-1}[(d_2 - d_1)\, g - P_{out}(t) H^{-1}](a^2 + b^2)^{-1} \quad (18)$$

The solution of Eq. (18) with the boundary condition $P(0) = 0$ is

$$P_{out}(t) = g\,(d_2 - d_1)\,[1 - \exp(-t\, \tau^{-1})] \quad (19)$$

where the 'characteristic time' (τ) (cf. Weinberger *et al*. 2006) has the following form:

$$\tau = [4\, \mu\, H\, a^{-2}\, b^{-2}\, d_1^{-1}\, g^{-1}(a^2 + b^2)] \quad (20)$$

Expanding the exponential series, neglecting terms higher than the second order, Eq. (19) becomes

$$P_{out}(t) = g\,(d_2 - d_1)\,(1 - t\, \tau^{-1}) \quad (21)$$

Substituting this value of $P_{out}(t)$ from Eq. (21) into Eq. (15), and neglecting the negative sign on the right hand side, the absolute value of the velocity, U_z (x,y,t), is obtained as

$$U_z(x,y,t) = 0.5\, g\, \mu^{-1}\, a^2\, b^2\,(d_2 - d_1)\,(a^2 + b^2)^{-1} \times (1 - x^2\, a^{-2} - y^2\, b^{-2})\,(1 - t\, \tau^{-1}) \quad (22)$$

For a circular cross-section, putting $a = b = y_0$, the radius of the circle; and $y_1 = (x^2 + y^2)^{0.5}$, the distance of the centre; the velocity profile, given by Eq. (22), simplifies to

$$U_z(y_1,t) = 0.25\, g\, \mu^{-1}(d_2 - d_1)\,(y_0^2 - y_1^2)\,(1 - t\, \tau^{-1}) \quad (23)$$

https://doi.org/10.1017/S001675680999077X Published online by Cambridge University Press

The 'characteristic time' (Weinberger *et al.* 2006), in this case, simplifies to

$$\tau = (8\,\mu\,H\,y_0^{-2}\,d_1^{-1}\,g^{-1}) \qquad (24)$$

Until Eq. (15), our derivations follow steps similar to Papanastasiou, Georgiou & Alexandrou (2000), and derivations from Eq. (16) until Eq. (22) follow Weinberger *et al.* (2006) while maintaining the physical boundary conditions appropriate for our problem. The extrusion parameters and the channel geometry of the diapirs are equated with the above fluid mechanical model as follows:

(x,y): coordinates of locations of known uplift rates on elliptical cross-section. These coordinates have been used in Eq. (22) and in Table 1.

U_z(x,y,t): velocity of the extruded salt at the coordinate (x,y) at instant 't', for extrusion through an elliptical cross-section. Symbol used in Eq. (22) and in Table 1.

τ: the 'characteristic time' of salt extrusion (see Weinberger *et al.* 2006 for definition), for the cases of both the elliptical and circular cross-sections of the diapir.

Symbols used in Eqs (20) and (24), respectively:

2a, 2b: length of the major and minor axes of the elliptical cross-section of the diapir; 8.5 km and 6.8 km, respectively, for the Hormuz salt diapir (Bruthans *et al.* 2006); symbols used in Eq. (22) and in Table 1.

$2y_0$: diameter of the circular cross-section. Symbol used in Eq. (23) and in Table 2. For the two diapirs, the diameters are considered as the major and minor axes of the elliptical cross-section of the Namakdan diapir: $2y_0 = 7$ km and 6.8 km.

U_z (y_1,t): velocity of the extruded salt at a distance y_1 from the centre of the diapir and at instant 't', for extrusion through a circular cross-section. Symbol used in Eq. (23) and in Table 2.

μ: dynamic viscosity of the salts of the two diapirs; symbol used in Eqs (20) to (24) and in Tables 1 and 2.

d_1, d_2: density of salt and that of the limestone, whose natural ranges are between 2.0–2.2 gm cm^{-3} and 2.37–2.8 gm cm^{-3}, respectively (Mizutani, 1984). This gives $d_{max\ diff} = (d_2 - d_1)_{max} = 0.8$ gm cm^{-3}. (for $d_1 = 2$ gm cm^{-3}, $d_2 = 2.8$ gm cm^{-3}) and $d_{min\ diff} = (d_2 - d_1)_{min} = 0.17$ gm cm^{-3} (for $d_1 = 2.2$ gm cm^{-3}, $d_2 = 2.37$ gm cm^{-3}). These values of '$d_{max\ diff}$' and '$d_{min\ diff}$' are used in $(d_2 - d_1)$ in Eqs (22) to (24), and in Tables 1 and 2 in calculating the 'μ' of salts.

H: length of the stem of the diapir; H = 10 km and 8 km for the Hormuz and Namakdan diapirs, respectively (Koop & Stonely, 1982; Bahroudi & Talbot, 2003).

t: span of diapirism for the Hormuz and Namakdan diapirs. $t = 10^4$ yrs (Bruthans *et al.* 2006).

https://doi.org/10.1017/S001675680999077X Published online by Cambridge University Press